The International Journal of Advanced Manufacturing Technology (2022) 121:6393–6406
https://doi.org/10.1007/s00170-022-09719-7

ORIGINAL ARTICLE

Tribological behavior of PTFE/Nomex/phenolic composite lubricant under cold forming condition in the bearing assembly process

Chengliang Hu[1,2] · Yue Zhuo[1,2] · Linlin Zhu[3] · Xiongrong Huang[3] · Hongyu Liu[3]

Received: 21 January 2022 / Accepted: 7 July 2022 / Published online: 22 July 2022

Abstract

The fabric composites, which are always used as a self-lubricant liner, also work as a forming lubricant during the assembly of the spherical plain bearings. Different from previous published works, the tribological behavior of polytetrafluoroethylene (PTFE)/Nomex/phenolic composite lubricant under cold forming condition in the bearing assembly process was investigated in details. A hybrid PTFE/Nomex fabric composite with a volume fraction of 1:3 coated with phenolic resin matrix sticking on a stainless steel 05Cr17Ni4Cu4Nb was prepared for the study. The ring with boss compression test (RCT-B) was selected as a tribometer, and a specific group of calibration curves were constructed by simulations with various friction factors. To obtain favorable tribological performance of the fabric-composite lubricant, the preparation parameters of the testing workpieces, including number of sandblasting cycles, curing time, and curing temperature, were optimized. To explore the lubricate limit of the optimal fabric-composite lubricant, the RCT-B tests with much larger reduction in height under much higher press speed were furtherly carried out. The failure modes of the fabric-composite lubricant, mainly including peel off, hysteresis, and delamination, were revealed. The failure mechanisms and the applicable limitation of the fabric-composite lubricant were finally discussed.

Keywords Fabric composites · Tribology behavior · Cold forming · Failure modes

1 Introduction

Cold forging is most common when parts are forged without heating the billet. It is a near net-shape manufacturing process. It is a cost-effective method to produce auto components such as shafts [1–3], gears [4–6], and other parts including inner race [7], outer race [8], and spark plug shell [9] in complex shape. Lubrication of the billets formed is critical to increase the life of the mating forging dies.

In the manufacture of spherical plain bearings, cold forging process is also used [10–12] in mass production. As for spherical plain bearings, hybrid fabric composites [13] are always employed as the self-lubricating liners [14, 15] to reduce friction and wear. In recent years, filler enhancement, surface modification, and the combined technologies have been proposed to improve the tribological properties of different fabric composites.

The addition of nano-titania [16], multiwalled carbon nanotubes [17], polystyrene functionalized graphene [18], graphene oxide [19], zirconium diboride particles [20], and milled pitch-based carbon fibers [21] can enhance the anti-wear ability of fabric composites, and the corresponding appropriate amount of different fillers for different composites has been determined. Furthermore, hybrids of graphite and MoS2 [22], nano-Si3N4 and submicron size WS2 [23], multiwalled carbon nanotubes and graphene oxide [24], boron nitride nanosheets and carbon nanotubes [25], single-walled carbon nanotubes and inorganic fullerene-like WS2 [26] were also used as fillers to improve the tribological performances of fabric composites. Various surface modification techniques, including cryogenic treatment [27], plasma treatment [28], chemical etching [29], ultrasonic radiation [15], chemical coating [30], and laser surface texturing [31],

✉ Chengliang Hu
clhu@sjtu.edu.cn

1 Institute of Forming Technology & Equipment, School of Material Science and Engineering, Shanghai Jiao Tong University, Shanghai 200030, China

2 National Engineering Research Center of Die and Mold CAD, Shanghai Jiao Tong University, Shanghai 200030, China

3 Shanghai Bearing Technology Research Institute, Shanghai 201800, China

have been developed to decrease the friction coefficient and wear rate of fabric composites. Recently, many efforts have been dedicated to investigate on the combined methods of surface treatment and filler reinforcement [32–34]. Therefore, the comprehensive performance of fabric composites including tribological properties has been improved.

Among these hybrid fabric composites, the polytetrafluoroethylene (PTFE)/Kevlar [35, 36] and PTFE/Nomex [37, 38] composites are always applied as the self-lubricating liners in bearing industry. Through finite element (FE) method and experiment, the dynamic distributions of the contact stress, wear depth and the worn morphology of the fabric liner were investigated [36]. To simulate the failure process of spherical plain bearings in the swinging wear condition, the 3D FE model was established based on Archard adhesion wear theory, and the wear mechanism of the fabric liner was revealed with experimental tests [39]. A simplified 2D FE model was created to predict the wear depth of the fabric liner [40]. The role of transfer film formation on the tribological properties of fabric composites in spherical plain bearing at low temperature is investigated in details [41]. Furthermore, a real case study about the failure reasons and wear mechanisms of a joint bearing in helicopter were analyzed, and the dominating phenomena were continuous generation, spalling, extrusion, and regeneration of the PTFE transfer film occurred between the inner ring and fabric liner [42].

As mentioned above, there are many excellent works about the tribological behaviors of self-lubricating fabric liners under working condition of bearings used in components, always by using the typical ball on disk or pin on disk testing methods. Actually, during the assembly of spherical plain bearings, the hardened inner ring acts as the inner die when the outer ring is cold deformed, and the fabric-composite liner sticking on the outer ring works as forming lubricant at that moment, as shown in Fig. 1. However, there is very little work on the tribological behavior in this cold assembled process. The present works only focus on the interface friction between the outer ring and forming dies lubricating with Molykote lubricant [43], and try to simulate the cold forming process for further optimization [44].

In this study, the tribological behavior of PTFE/Nomex fabric composites under cold forming condition was tried to be investigated. In the following section, the preparation of the testing workpiece according to the manufacturing process of spherical plain bearings is first described, followed by the key steps of the preparation process. In Sect. 3, the ring with boss compression test (RCT-B) proposed in previous work [45] using as a tribometer for cold forming is briefly introduced, and the corresponding calibration curves are constructed by the FE method using the tested data of material 05Cr17Ni4Cu4Nb which is used to make the outer ring in the spherical plain bearing. In Sect. 4, the key process parameters, including number of sandblasting cycles, heating curing time, and curing temperature, are orthogonally optimized to achieve a lower shear friction factor, and the determined friction factor could be used to simulate the cold forming process of the spherical plain bearing. In Sect. 5, the effects of the reduction in height and press speed on the deformation and damage-prevention properties of the optimized fabric-composite lubricant are experimental tested further, and the failure mechanisms and limitation of the fabric composites working as lubricant in cold forming are discussed. Finally, the conclusions drawn from this research are summarized in Sect. 6.

2 Preparation of the testing workpiece

To carry out the experimental works for the tribological study, the testing workpieces were prepared according to the actual manufacturing process of the spherical plain bearing. In the first step, a hybrid PTFE/Nomex fabric composites

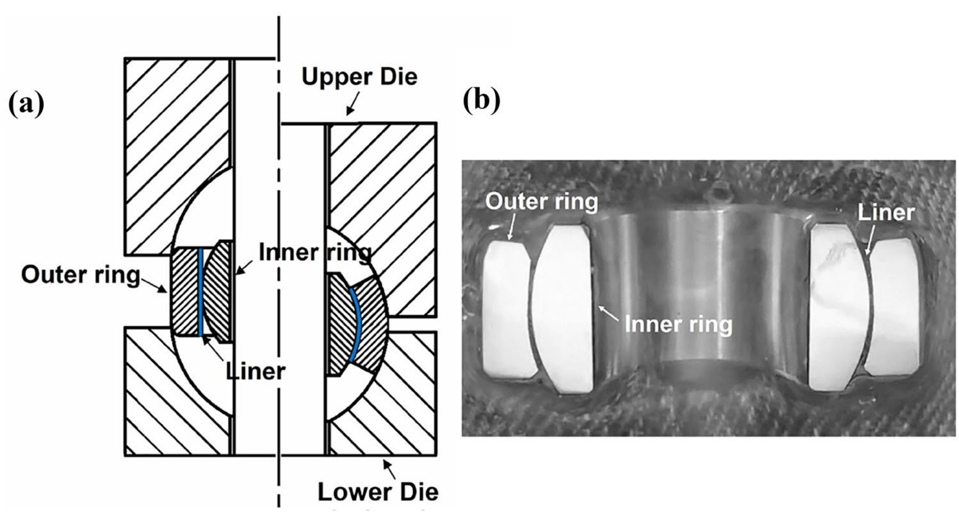

Fig. 1 Assembly of spherical plain bearing: **a** cold extrusion process and **b** cross section of assembled part

with a volume fraction of PTFE to Nomex:1:3 was roll-coated with phenolic resin matrix, and the mixed composite was precured under a plate curing press. Secondly, the stainless-steel ring specimens were machined from raw bars after heat treatment as required for outer ring in spherical plain bearing, and the specimen surfaces where the composite was to be pasted were sandblasted accordingly. Finally, the mixed composites were pasted to the end surfaces of the ring specimens by using phenolic resin adhesive, and the curing process proceeded under clamping pressure. Once the curing process had been completed, the testing workpiece for the following tribological tests was obtained.

2.1 Precuring of fabric composites

The fabric was composed of PTFE fibers (weft) and Nomex fibers (weft and warp), and a plain weave shown in Fig. 2a was adopted. The diameter of the PTFE and Nomex fibers was 22.44 and 18.06 μm, their breaking elongation was 19.10% and 30.06%, and their initial modulus was 20.35 and 106.30 cN/dtex, respectively. Once precuring had been completed, the mixed composites was formed with hybrid PTFE/Nomex fabric and phenolic resin matrix, as illustrated in Fig. 2b. The thickness of the composite lubricant could be controlled in the range of 0.38–0.42 mm.

2.2 Sandblasting of the stainless-steel specimen

Martensitic stainless steel (05Cr17Ni4Cu4Nb) was selected, and its chemical composition was C (0.07 wt%), Si (1.00 wt%), Mn (1.00 wt%), S (0.03 wt%), P (0.03 wt%), Cr (17.50 wt%), Ni (5.00 wt%), Cu (5.00 wt%), and Nb (0.45 wt%). As shown in Fig. 2, the stainless steel was heat treated according to the heat treatment process for the outer ring of spherical plain bearings. In the solution process, the received bar was heated up to 1030 °C by employing three heat preservation stages at 650 °C, 850 °C, and 1030 °C and then cooled to room temperature in 15 min. In the aging process, the round bars were heated to 620 °C, maintained at that temperature for 4 h, and then cooled. In the microstructure after heat treatment (Fig. 3), the retained and precipitated granular carbides could enhance the dispersion strengthening effect and improve the comprehensive mechanical properties.

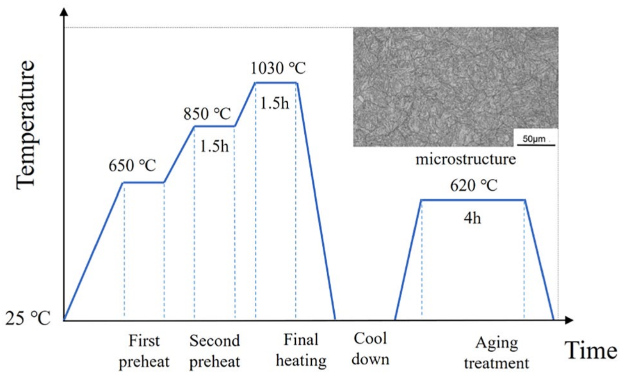

Fig. 3 Heat treatment process and obtained microstructure

After being machined from the heat-treated bars, the top and bottom surfaces of the ring specimens were sandblasted with 24 emeries by using an ACEOP-II shot peening machine. An intermittent shot peening mode was adopted at an interval of 10 s with a spray gun in 6-mm diameter. The flow rate was 2.0 m^3/min, and the shot pressure was set at 0.50 MPa. The ring specimens were slowly sandblasted using circular movements, and various surface topographies could be obtained by differing the number of cycles.

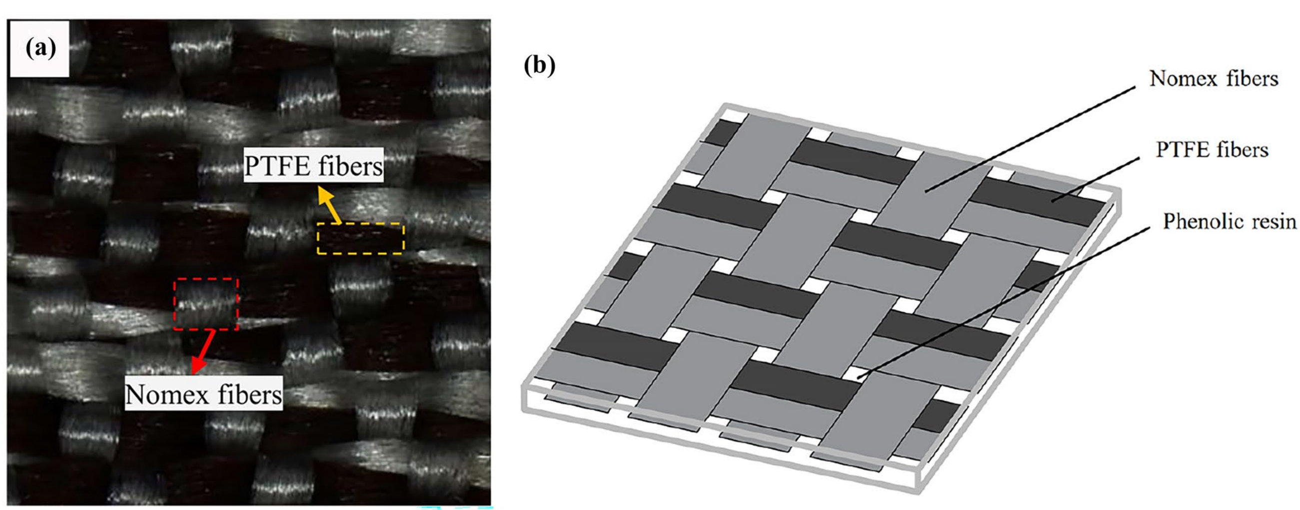

Fig. 2 Weave structure (**a**) and schematic (**b**) of the fabric composite. PTFE and Nomex fibers are shown in black and gray with a volume fraction of 1:3

2.3 Final curing process the workpiece

To realize the final curing process, a simple clamping setup shown in Fig. 4 was adopted. The ring specimen with the PTFE/Nomex/phenolic composites covered on the top and bottom end surfaces was clamped between the PTFE and steel plates. The clamping pressure was maintained at around 2 MPa by tightening four nuts synchronously. The curing temperature was set at 100–160 °C, and the curing time was 1–3 h. In this process, the phenolic resin was cured gradually, and the mixed composites were well pasted on the end surfaces of the ring specimen. Then, the testing workpieces for later tribological evaluation were prepared.

3 Tribological testing method

Different from the typical mechanical friction, here is the friction between the inner ring and the fabric liner when the bearing is running, the friction in metal forming, here is the friction at interface between the inner ring and the fabric liner when the outer ring is cold formed during the assembly, is always involved with very high contact pressure to plasticize the workpiece material [46]. What is more, new surface of workpiece generates during metal forming, and the surface enlargement depending on the workpiece shape [47] is relatively larger. As for the third index of tribological load, the relative velocity in mechanical friction depends on the running speed of components, while the relative velocity between die and workpiece is mainly determined by the forming speed.

To characterize tribological behavior in cold forming, more than 20 different tribotests for cold forging have been proposed [48]. The ring compression test, which was firstly proposed by Kunogi [49] and further developed by Male and Cockcroft by introducing a set of calibration curves [50], has been one of the most commonly used methods because of its convenience. An alternative method named as RCT-B was put forward [45], where the outer diameter of boss of ring specimen before and after deformation could be measured easily and precisely, which could enable more accurate measurement of friction conditions. Therefore, the established RCT-B method in the lab is adopted for the tribological tests of the PTFE/Nomex/phenolic composites under cold forming condition.

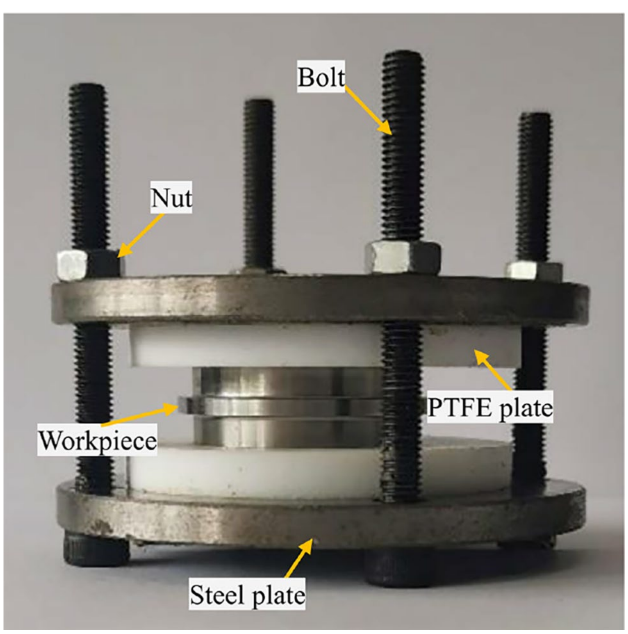

Fig. 4 Elements of the clamping setup

3.1 Material flow curves

To quantify the friction factor in cold forming condition, a corresponding group of calibration curves needs to be constructed according to simulation results. To obtain the material flow curves for the simulation, a group of uniaxial tensile tests of 05Cr17Ni4Cu4Nb stainless steel, which was treated by the same heat treatment process mentioned in Sect. 2.2, were performed at room temperature. According to the testing data, the following mechanical property parameters were determined: Young's modulus, 198.70 GPa; Poisson's ratio, 0.29; yield strength, 727.12 MPa; and tensile strength, 966.23 MPa.

As shown in Fig. 5, the stress–strain curves from three tensile samples were plotted, and the data curves of the three samples (C1, C2, and C3) were collected using strain gage and load cell. To describe the hardening behavior of the

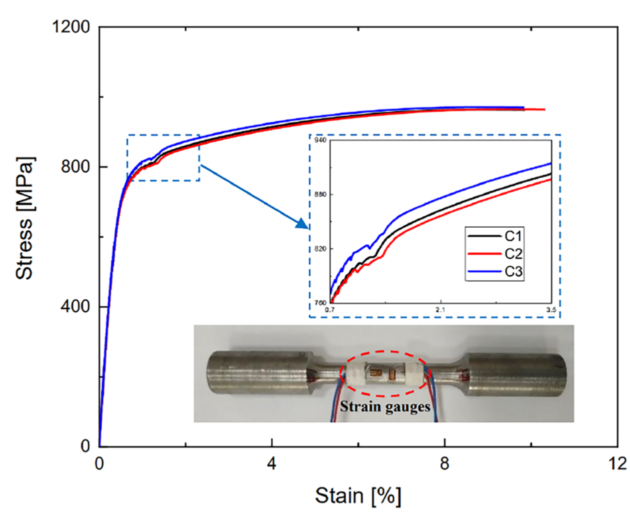

Fig. 5 Stress–strain curves of the 05Cr17Ni4Cu4Nb stainless steel

05Cr17Ni4Cu4Nb stainless steel, a Swift-Voce type law, which is a combination of the unsaturated Swift type law and the saturated Voce type law, was selected. The combined material model was employed because it may improve the prediction accuracy of the material hardening behavior [51]. On the basis of uniaxial tensile test data, the values of various parameters in the selected Swift-Voce type law could be determined by fitting. The specific hardening law is derived as follows:

$$\sigma = 0.0021(\varepsilon + 0.0006)^{2.50} + 0.07 \times [841.15 + 315.84 \times (1 - e^{-19.67\varepsilon})] \quad (1)$$

3.2 Calibration curves

The fitted Swift-Voce type law was input the FE model of the compression process of the ring with boss with a pressing speed of 1.65 mm/s at room temperature. The basic size ratio of the outer diameter, inner diameter, and height of the ring specimen was 6:3:2, as shown in Fig. 6. The nominal dimensions of the outer diameter, inner diameter, height, as well as the height and width of the outer boss were 30.00, 15.00, 10.00, 2.00, and 2.00 mm, respectively.

Simulations with various friction factors, obeying the shear friction rule, were performed to construct the calibration curves. As shown in Fig. 7, the relationship lines between the reduction in outer diameter of the boss (denoted as R_B) and the reduction in height (denoted as R_H) under different friction factors are determined according the specified calculation method in previous work [45]. The variation in the outer diameter of the outer boss for every height reduction was extracted from the simulation results, and the specific calibration curves within the friction factor ranged from 0 to 0.3 were constructed. Under the reduction in height of 30%, when the friction factor was 0, 0.1, and 0.3, the straight, concave, and convex profiles of the inner diameter were as expected, as illustrated in Fig. 7.

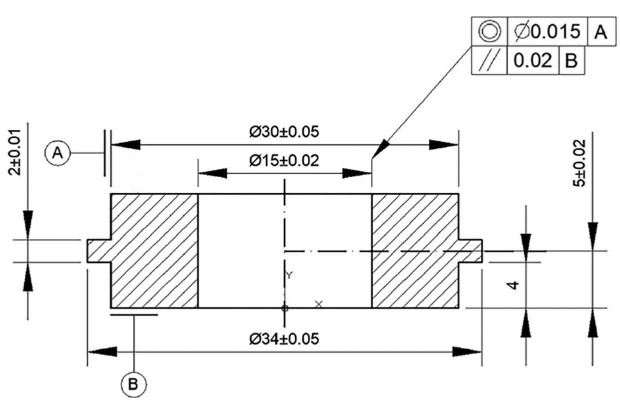

Fig. 6 Dimensions of the ring specimen

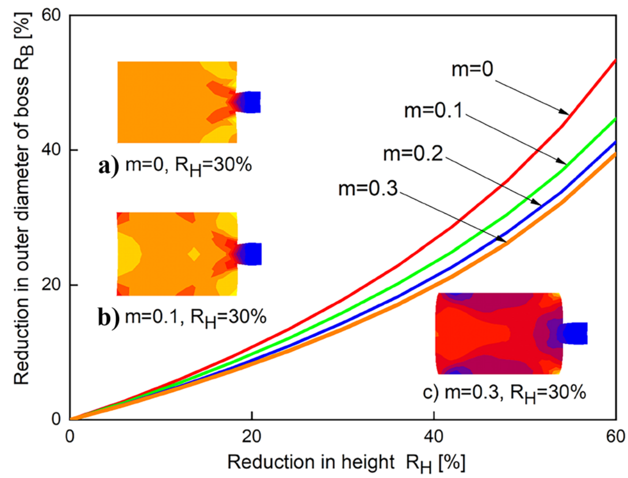

Fig. 7 Calibration curves of four different friction factors (i.e., $m=0$, 0.1, 0.2, and 0.3) and the straight (**a**), concave (**b**), and convex (**c**) profiles of the inner diameter of the ring

4 Optimization for minimum friction factor

In the manufacturing process of spherical plain bearings, the outer ring stick with the mixed PTFE/Nomex/phenolic composites is always firstly prepared before assembly using cold extrusion process. As described in Sect. 2, three parameters including number of sandblasting cycles, heating curing time, and curing temperature can be adjusted during the aforementioned preparation process. Therefore, the preparing process of the mixed composites will be optimized to achieve better lubrication performance based on the RCT-B tests.

4.1 Design schemes

As shown in Table 1, three controllable process parameters, namely number of sandblasting cycles, heating curing time, and curing temperature, with three levels were established according to the actual process. Correspondingly,

Table 1 Controlling parameters and their levels

Parameter	Curing time t (h)	Curing temperature T (°C)	Sandblasting cycles N
Level 1	1	100	3
Level 2	2	130	5
Level 3	3	160	7

Table 2 Testing schemes based on orthogonal design

Scheme	t (h)	T (°C)	N	Evaluation index $\theta\times100\%$
1	1	130	7	45.848
2	1	100	3	46.770
3	1	160	5	48.112
4	2	130	5	47.001
5	2	100	7	47.237
6	2	160	3	48.222
7	3	130	3	47.141
8	3	100	5	48.038
9	3	160	7	46.787
$k1$	46.910	46.663	46.624	
$k2$	47.487	47.349	47.738	
$k3$	47.322	47.707	47.717	
Range	0.577	1.044	1.093	

nine schemes with various process parameters based on the orthogonal design method representing nine different conditions are given in Table 2. Subsequently, four workpieces for each scheme were prepared, and the RCT-B tests were conducted on a H1F200S servo press. The press speed was set at 1.65 mm/s, and four reductions in height (approximately 20%, 22.5%, 25%, and 30%) were employed.

4.2 Evaluation index

After all the RCT-B tests in Table 2 were completed, the outer diameter of the outer boss and the height of the ring workpiece were measured. The reduction in outer diameter of boss and the reduction in height were calculated. The corresponding data were plotted on the calibration curves, as shown in Fig. 8. The data points are relatively scattered on the diagram, suggesting the friction condition was considerably affected by the selected process parameters.

To facilitate the subsequent optimization, the ratio between the reduction in outer diameter of the boss and the reduction in height was first calculated for each compressed workpiece, and then the average ratio of four testing workpieces in each scheme was defined as an evaluation index θ, as summarized in Eq. (2). The larger the θ value, the smaller the friction factor and the more favorable the lubricating condition at the interface between the testing workpiece and the compression tools. All the values of evaluation index in different schemes are listed in Table 2.

$$\theta = \frac{1}{4}\Sigma R_{\mathrm{B}n}/R_{\mathrm{H}n}, \tag{2}$$

where n is the number of the testing workpiece, $R_{\mathrm{B}n}$ is the reduction in outer diameter of boss corresponding to the nth workpiece, and $R_{\mathrm{H}n}$ is the reduction in height of the nth workpiece.

4.3 Optimal results

By employing the Taguchi method, the mean values $k1$–$k3$ of the evaluation index θ of every process parameter at the three levels were calculated and recorded in Table 2. Regarding the curing temperature, the θ value was first decreased and then increased up to the maximum at the third level. As for curing time and number of sandblasting cycles, the θ values first increased and then decreased, and the maximums were reached at the second level. Thus, the optimized specific values of all the process parameters were determined: number of sandblasting cycles = 5, curing time = 2 h, and curing temperature = 160 °C.

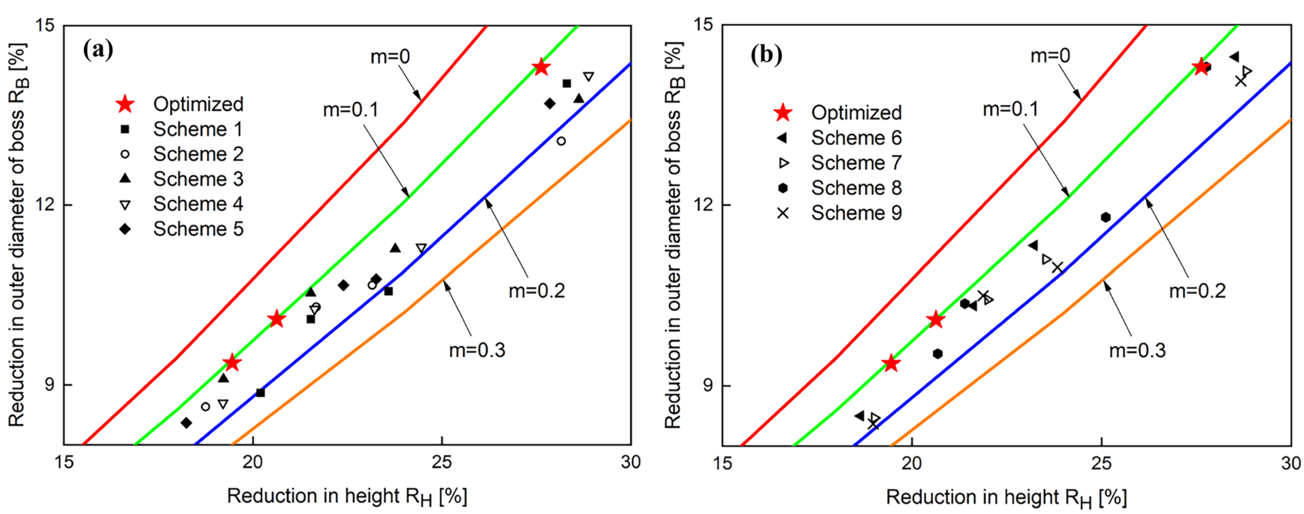

Fig. 8 Testing results: **a** schemes 1–5 and optimized scheme; **b** schemes 6–9 and optimized scheme

Based on the optimal process parameters, three testing workpieces were prepared and also evaluated by the RCT-B method. Similarly, the relative reduction in the outer diameter of the boss and reduction in height were obtained and plotted in Fig. 7. After optimization, the evaluation index θ reached 49.62%, and it was larger than that of all the sampling schemes, which suggests the optimization process was successful. From Fig. 7, the friction factor of the optimal scheme could be calibrated as 0.1. In addition, the plotted data points fit the calibration curve of $m = 0.1$ well, which indicates favorable stability of the mixed composite as a lubricant in cold forming after optimization.

5 Limitation analysis of the mixed composites as forming lubricant

As mentioned above, the preparation process of the mixed PTFE/Nomex/phenolic composites working as a lubricant for cold forming process has been optimized by the RCT tests under a lower forming speed (1.65 mm/s) and relatively smaller deformation degree (less than 30% of reduction in height). So, it will be interesting to find out the lubricate limit of the optimal mixed composites in cold forming. Here, the macro and micro status of the surface state of the fabric-composite lubricant after deformation will be furtherly investigated, and the unique non-uniformity, non-continuity, and complexity of failure mode of the mixed composites will be discussed.

In this condition, 6 testing schemes with a maximum reduction in height of 43.825% under larger press speeds of 16.50 and 41.25 mm/s were first tried. As shown in Table 3, the average surface expansion ratio of the end surface of testing workpiece in each scheme was calculated; the maximum value reached 1.595. The surface expansion ratio, which also can reflect the ability of the mixed composite to expand along with the surface of the ring specimen, can be used as an index to evaluate the reliability of the fabric-composite lubricant.

Table 3 First tried tests

Scheme	Press speed v (mm/s)	Reduction in height R_H (%)	Surface expansion ratio	Status of lubricant
S1	16.50	24.348	1.254	Good
S2	16.50	29.123	1.331	Good
S3	16.50	34.282	1.406	Good
S4	41.25	36.464	1.411	Good
S5	41.25	41.057	1.510	Good
S6	41.25	43.825	1.595	Good

As shown in Fig. 9, no visible surface defects could be observed by naked eyes. Here, the "good" was recorded for the status of the fabric-composite lubricant in Table 3. Definitely, the fabric-composite lubricant expands along the end surface of the ring specimen as the reduction in height increased. The vertical load acts on the phenolic resin in direct contact with upper die to promote it to move along the radial direction on the surface of the ring specimen. The strain difference between the phenolic matrix and the PTFE and Nomex fibers on the contact surface is formed, resulting in interfacial shear stress to make the fibers have the tendency of sliding, while the chemical bonding force and mechanical interlocking force between the fibers and matrix limit their relative motion.

Before compression, the existence of several voids in which bundles of fibers interweave demonstrates poor wettability of phenolic resin to fabric, which is detrimental for mechanical properties and wear resistance of composite, as depicted in Fig. 10a. After compression of the workpieces, the polymer macromolecules were compressed to smooth plane, and the initial micro gaps at the boundaries were generally filled. The matrix bonded well with the fabric despite a small number of matrix cracks were observed, as depicted in Fig. 10b. Overall, the surface of the fabric composite retained favorable integrity and could exert a lubricating effect during the stainless-steel deformation.

To investigate failure modes of the fabric-composite lubricant, the RCT-B tests under much larger reduction in height and much higher press speed would be furtherly performed. The effects of the reduction in height and the press speed would be investigated in details. During the further experimental tests, the load-time curves recorded by the press were extracted, and the contact pressure between the tool and the workpiece with the fabric-composite lubricant was calculated as the maximum load divided by the end surface area of the workpiece after compression of each test.

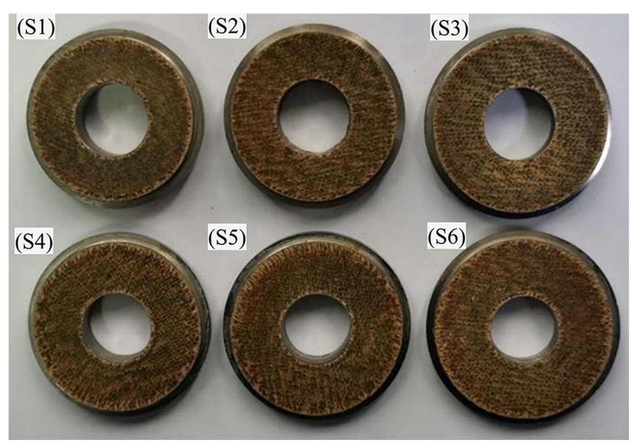

Fig. 9 The compressed workpieces corresponding to schemes S1–S6

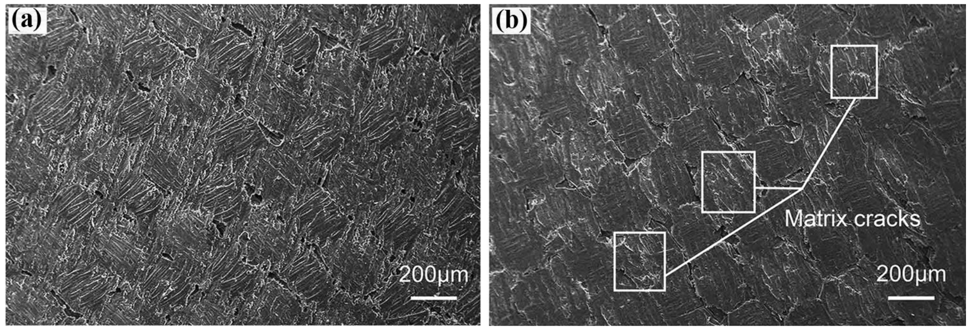

Fig. 10 Surface microscopic photographs: **a** before and **b** after deformation of scheme S1

Table 4 Tests under different reduction in height

No	Press speed v (mm/s)	Reduction in height R_H (%)	Status of lubricant
1	82.50	44.402	Good
2	82.50	45.619	Good
3	82.50	48.673	Good
4	82.50	54.220	Hysteresis
5	82.50	56.164	Hysteresis
6	82.50	57.286	Hysteresis + peel off

Meanwhile, the temperature of the workpiece during the testing process was tried to be captured by a forward-looking infrared thermal imager, and the maximum temperature of each test was recorded for later analysis.

5.1 Effect of the reduction in height

To investigate the effect of the reduction in height, different test schemes were designed with the reductions in height from 44.402 to 57.286% at a press speed of 82.50 mm/s, as listed in Table 4. The surface expansion ratio was increased as fast as the reduction in height was increased, and the maximum value reached 2.0, as shown in Fig. 11a. The contact pressure was increased gradually as the reduction in height as expected, cause that it is always increased as the degree of plastic deformation due to the strain hardening effect. The average contact pressure was increased from 962.52 to 1063.40 MPa, as shown in Fig. 11a. In cold forming, part of the plastic deformation work is transformed into heat energy, and the temperature of the workpiece is positively correlated with the degree of deformation. Here, the highest temperature of the tested specimen was 156.5 °C, as shown in Fig. 11b.

As shown in Fig. 12, the representative local appearance of the workpiece surface after compression with reduction in height of 44.402%, including the regions near the inner diameter, the middle, and near the outer diameter of the ring workpiece, was observed by a microscope. The different state of phenolic resin at three regions along the radius of workpiece was presented. As reported by Male and Depierre [52], there is a so called "neutral plane" during the ring compression, and the material flows both

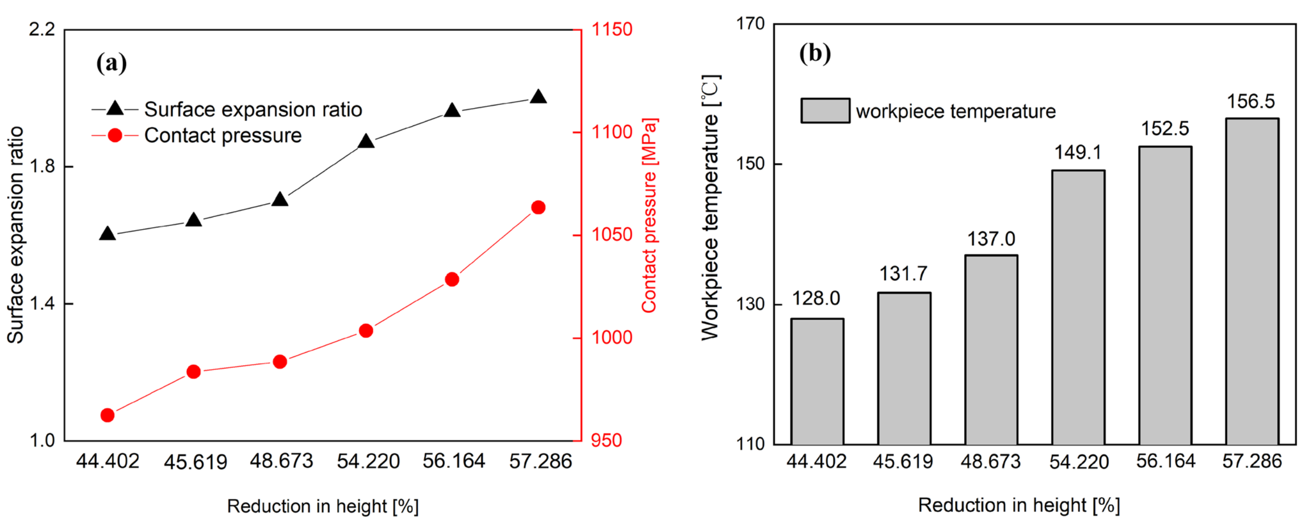

Fig. 11 The relationship of surface expansion ratio and contact pressure (**a**), and workpiece temperature (**b**) with the reduction in height

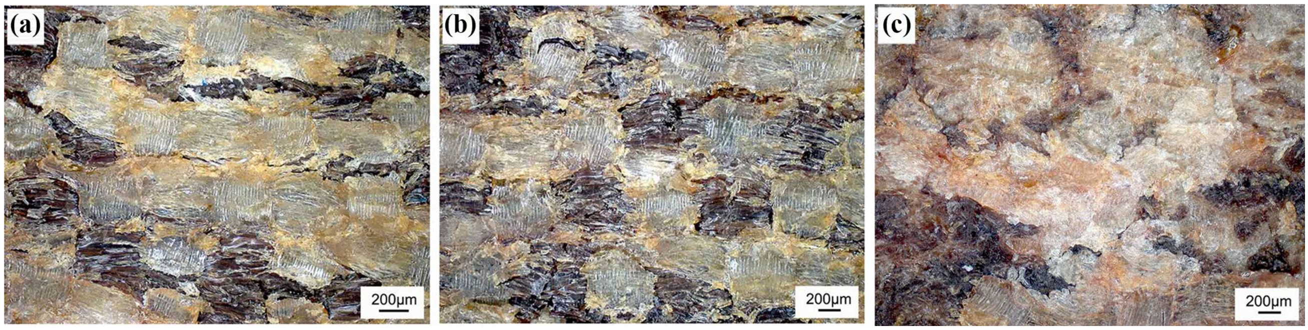

Fig. 12 Local appearance of the workpiece surface after compression with reduction in height R_H=44.4%, including the region near the inner diameter (**a**), the middle (**b**), and near the outer diameter (**c**) of the ring

inward and outward from the plane under high friction while the material main flows outward under lower friction along the radial direction. In this case, the determined friction factor of the fabric-composite lubricant was 0.1, so the material mainly flowed outward. Therefore, during the compression the semi-solid phenolic resin was squeezed outwards along the radial direction with the material flow of stainless-steel specimen, the original uniform distribution was changed to random distribution (Fig. 12a, b), and much more phenolic resin was accumulated on the outer edge, as seen in Fig. 12c.

Regarding this random distribution phenomenon, one of the main contributions comes from the radially distributed interfacial shear stress acting on the fabric composite which was woven in a regular array (Fig. 2). Another contribution should be the different bonding properties to phenolic resin matrix between the PTFE and Nomex fibers, the interface between the PTFE fibers and phenolic resin matrix seems relatively easy to debond in the compression process. What is more, the color of accumulated phenolic resin layer in Fig. 12c shows a slight char in somewhat [53]. As analyzed in Ref [54], phenolic resins are relatively stable up to about 200 to 250 °C and start to char slowly at the elevated temperature. During the test, the captured temperature around 128 °C (Fig. 11) was relatively lower because the higher flash temperature [55] was not measured and heat transfer from billet to tools before the temperature capturing.

As further observed in Fig. 12b, some PTFE fibers in brown were exposed because of relatively smaller bonding strength with the matrix, and the crack perpendicular to the direction of the fibers locally occurred due to interfacial shear stress [56]. When the reduction in height increased, the local cracks of fibers were coupled and extended to form macroscopic and continuous cracks distributed along the circumferential direction of the ring specimen, intensifying the further deterioration of the fabric composite. Therefore, fish-scale cracks appeared with a height in reduction of 45.619%, as shown in Fig. 13a. Excessive pulled-out and cut-off fibers and numerous cracks with fish-scale morphology presented on the surface of the fabric-composite lubricant. As observed in Fig. 13b, the serious broken and deboned fibers showed like a hole. Some wear debris could be found around the hole, and the broken fibers presented a natural bending shape.

Under the conditions of microscopic observation, a lot of small cracks are there. However, in macro-scale, the fabric-composite lubricant maintains integrity and protects the end faces of the stainless-steel specimen, providing lubrication effect during compression process (Fig. 14a–c).

When the reduction in height increased to 54.220%, the fabric-composite lubricant could not adequately cover the ring specimen (Fig. 14d), and the outer edge of the stainless-steel specimen was exposed. The hysteresis phenomenon reflects that the surface expansion of the fabric-composite

Fig. 13 SEM observation of composite surface at the height in reduction of 45.619%: **a** fish-scale cracks and **b** hole

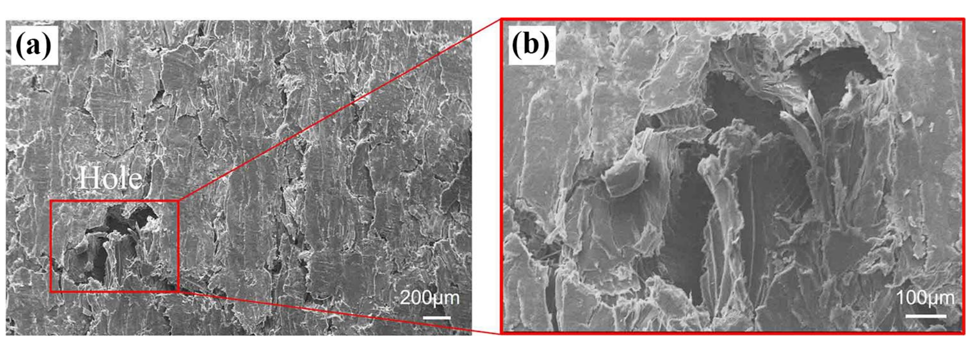

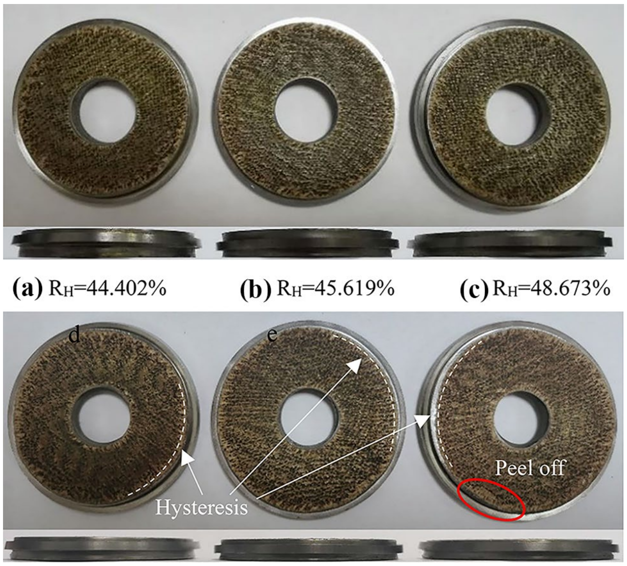

(a) R_H=44.402% **(b)** R_H=45.619% **(c)** R_H=48.673%

(d) R_H=54.220% **(e)** R_H=56.164% **(f)** R_H=57.286%

Fig. 14 End faces and sides of workpiece after deformation under various reductions in height at a press speed of 82.50 mm/s

lubricant could not keep up with that of stainless steel at the interface. As shown in Fig. 14e, the hysteresis phenomenon became more serious when the reduction in height reached 57.286%, and the shining outer edge on ring specimen was observed, resulting in metal-to-metal direct contact between the tool and the specimen. As the reduction in height increased further, significant hysteresis phenomenon and local peel off occurred, as shown in Fig. 14f. Regarding the cause of the peel off defect, the fine crack defects formed during the compression were propagated by further deformation especially in the area of high shearing stress. In the peel-off zone, the severe friction condition could be generated because of the direct metal-to-metal contact.

5.2 Effect of press speed

As discussed in Sect. 5.1, the variation of the reduction in height of the RCT-B tests, followed with the change of the contact pressure and the surface expansion ratio, has been studied. Here, the other characteristic parameter of tribological loads, the relative velocity between tool and workpiece, will be further studied. Definitely, the relative velocity between tool and workpiece could be directly changed by the press speed. To investigate the effect of press speed, test schemes were arranged with press speeds from 107.25 to 346.50 mm/s at a reduction in height of 40.684%, as given in Table 5. The captured temperatures of workpieces after compression fluctuated between 134.3 °C and 138.2 °C. It was dominated by the reduction in height, and the effect of the press speed was not significant. The similar slight variation of the measured contact pressure

Table 5 Tests under different press speeds

No	Press speed v (mm/s)	Reduction in height R_H (%)	Contact pressure (MPa)	Status of lubricant
1	107.25	40.684	947.90	Good
2	132.00	40.684	949.69	Good
3	165.00	40.684	952.37	Good
4	247.50	40.684	939.85	Peel off
5	288.75	40.684	947.90	Peel off
6	313.50	40.684	941.64	Delamination
7	330.00	40.684	938.06	Delamination
8	346.50	40.684	946.11	Delamination

mainly depended on the reduction height, varied from 938.06 to 952.37 MPa, was recorded in Table 5. From the appearance of the compressed workpieces, there were no macro defects on the surface of the fabric-composite lubricant even when the press speed reached 165 mm/s.

When the press speed was set at 247.50 mm/s, a large amount of fabric-composite lubricant peeled off at the outer edge of the ring specimen, resulting in a thickness reduction and a different surface topography at the damaged zone, as seen from Fig. 15a. According to the SEM image in Fig. 16a, the peel off zone seems smoother after shearing and the other zone shows more cracks. A higher forming speed will introduce a larger relative velocity at the interface, and a larger sliding speed will result in a larger coefficient of friction [57], and the frictional stress will also become larger, then severe shearing stress generates at the interface. The accumulation of fiber cracks and the debonding between fibers and matrix was enhanced by high-level shear stress, and then a large area of peel off took place.

At a higher press speed of 313.50 mm/s, the lubricant layer separated from the steel specimen along the circumference of a specific radius, and the delamination phenomenon occurred, as shown in Fig. 15b. When the press speed was increased up to 346.50 mm/s, delamination became more prominent,

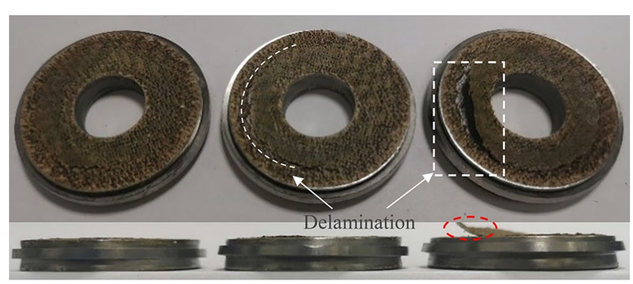

(a) v=247.50mm/s **(b)** v=313.50mm/s **(c)** v=346.50mm/s

Fig. 15 End faces and sides of compressed workpiece under various press speeds at a reduction in height of 40.68%

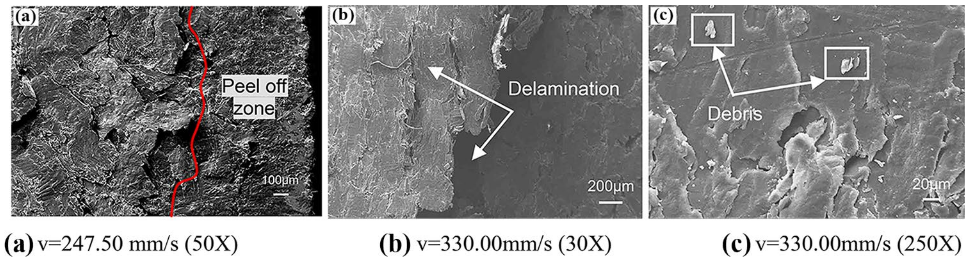

Fig. 16 SEM images of composite surface under various press speeds, including local peel off zone (**a**), separation of lubricating layer and the adhesive surface (**b**), and debris (**c**)

and a large area of metal was exposed due to the considerable warping of the lubricating layer, as shown in Fig. 15c. In the outer area of the ring specimen, the fabric-composite lubricant layer was sheared off and broken into pieces and was squeezed outside the surface.

When the specimen surface compressed with a high press speed of 330.00 mm/s was investigated, the significant local delamination phenomenon was easily observed, as shown in Fig. 16b. The delamination becomes one of the major failure modes endangering the reliability of fabric-composite lubricants [58]. The mechanism of delamination is relatively complex, involving highly anisotropic, high stress intensities, and interface discontinuities. Interlaminar stress is a major component of the complex three-dimensional stress leading to delamination, which is caused by the mismatch of Poisson effect caused by different fiber orientations [59, 60]. High relative speed at the interface increases the risk of delamination defects because of the high level of interlaminar stress. Due to the inherently weak interfacial strength and fracture toughness of the matrix, delamination tends to occur in the resin enriched area between the fabric composite lubricant and the ring specimen, but can also occur at geometric discontinuities of the fibers. Delamination results in the appearance of a large number of abrasive particles, mainly including PTFE and Nomex fiber debris, resin, and trace metal abrasive debris (see Fig. 16c), among which small-size PTFE debris can easily be trapped in surface pits as a secondary source of lubricant for repairing damaged surfaces [61]. When severe hysteresis or delamination occurs during the deformation process, the integrity of the fabric-composite lubricant is severely damaged. The corresponding lubricating effect is weakened, and a non-uniform friction will be created, resulting in an inclination of the outer boss of the ring specimen. The strong inclination could be easily found in Fig. 15c, and this inclination of the outer boss was already proved to be indicative of poor friction condition in cold forging [45].

6 Summary and outlook

The spherical plain bearings are always assembled in mass production by using cold extrusion process, and the fabric-composite liner sticking on the outer ring also works as a lubricant during the cold forming of the outer ring. Therefore, the tribological behavior of a PTFE/Nomex/phenolic composite in cold forming condition was investigated using the RCT-B method. To guide the application in industry, the lubricate limit and the failure modes were also explored. The main conclusions can be summarized as follows:

1. The average ratio of the reduction in outer diameter of the boss to the reduction in height was defined as the evaluation index, and the adjustable parameters including number of sandblasting cycles, curing time, and curing temperature were selected as design variables, then an optimal group of process parameters were determined: number of sandblasting cycles = 5, curing time = 2 h, and curing temperature = 160 °C. After optimization, the maximum evaluation index reached 49.62, and the friction factor of the fabric-composite lubricant was stabilized at 0.1.
2. To explore the lubricate limit of the fabric-composite lubricant, the tribological loads including contact pressure, surface expansion ratio, and the relative velocity between tool and workpiece were changed by the variation of the reduction in height and press speed. From the tested results, the fabric-composite lubricant could keep favorable surface integrity when the reduction in height is smaller than 48.6% and the press speed is lower than 165.00 mm/s. In these cases, although there are some local cracks of fibers but no visible surface defects could be observed by naked eyes, and the end faces of the stainless-steel specimen are well protected.
3. Three mainly failure modes, including hysteresis, peel off and delamination, were found on the fabric-composite lubricant in cold forming. The hysteresis phenomenon reflects that the surface expansion of the fabric-composite lubricant could not keep up with that of stainless steel at the interface. The peel off defect is mainly caused by that the fine cracks formed during the compression are propagated by further deformation especially in the area of high shear stress. The larger the relative speed at the interface, the higher the interlami-

nar stress generates, and the higher the risk of delamination defects on the fabric-composite lubricant.

4. Considering the limitation of the PTFE/Nomex/phenolic composite working as lubricant in cold forming, it would be interesting to find out the solution to improve the comprehensive tribological performance to endure higher contact pressure and larger surface expansion. Due to the facts that fine cracks could be found on the fabric-composite lubricant during the cold compression, the effect of pre-strain on the wear property in service of the fabric composites which are applied as the self-lubricant liner in the spherical plain bearings will be investigated in the upcoming works.

Author contributions CH: conceptualization, supervision, writing—review and editing, funding acquisition. YZ: methodology, investigation, data curation, writing—original draft. LZ: investigation, data curation, validation. XH: investigation, data curation, project administration. HL: conceptualization, supervision.

Funding This work was supported by the National Natural Science Foundation of China (No. 51475294).

Declarations

Ethics approval Not applicable.

Consent to participate Not applicable.

Consent for publication Not applicable.

Competing interests The authors declare no competing interests.

References

1. Bulzak T, Tomczak J, Pater Z (2021) A comparative analysis of hot and cold flashless forging of a stepped shaft using vertically-parted dies. Int J Adv Manuf Tech 116(7):2521–2530. https://doi.org/10.1007/s00170-021-07542-0
2. Jo AR, Jeong MS, Lee SK, Moon YH, Hwang SK (2021) Multi-stage cold forging process for manufacturing a high-strength one-body input shaft. Materials (Basel) 14(3):532. https://doi.org/10.3390/ma14030532
3. Ossenkemper S, Dahnke C, Tekkaya AE (2019) Analytical and experimental bond strength investigation of cold forged composite shafts. J Mater Process Tech 264:190–199. https://doi.org/10.1016/j.jmatprotec.2018.09.008
4. Rohrmoser A, Hagenah H, Merklein M (2021) Adapted tool design for the cold forging of gears from non-ferrous and light metals. Int J Adv Manuf Tech 113:1833–1848. https://doi.org/10.1007/s00170-020-06449-6
5. Liu Z, Zhou J, Qu Z, Wang X, Liang Q, Feng W (2021) A precision sizing method for cold extruded sun gear with internal-external tooth shapes. Int J Adv Manuf Tech 115:3331–3344. https://doi.org/10.1007/s00170-021-07405-8
6. Weiß A, Deliktas T, Liewald M, Missal N (2020) Cold forging of gear components by a modified Samanta process. Forsch Ingenieurwes 84:215–221. https://doi.org/10.1007/s10010-020-00403-4
7. Ku TW, Kang BS (2014) Tool design for inner race cold forging with skew-type cross ball grooves. J Mater Process Tech 214:1482–1502. https://doi.org/10.1016/j.jmatprotec.2014.02.021
8. Ku TW, Kim LH, Kang BS (2014) Process simplification of multi-stage forging for the outer race of a CV joint. Mater Manuf Process 29:85–92. https://doi.org/10.1080/10426914.2013.792432
9. Al-Shammari MA, Zedan LY, Al-Shammari AM (2018) FE simulation of multi-stage cold forging process for metal shell of spark plug manufacturing. 1st International Scientific Conference of Engineering Sciences-3rd Scientific Conference of Engineering Science 209–214
10. Woodhead J, Booker JD, Truman CE (2014) Impact of geometric variation on the performance of cold formed bearings. Proceedings of the First International Symposium on Robust Design, Copenhagen, Lyngby, Denmark 159–170
11. Woodhead J, Booker JD (2013) Modelling of nosing for the assembly of aerospace bearings. In: Ventura CE, Crone WC and Furlong C (Eds.) Experimental and applied mechanics, New York pp. 327–337. https://doi.org/10.1007/978-1-4614-4226-4_38
12. Orsolini A, Booker JD (2012) Modelling capabilities required for the double nosing process in the assembly of spherical plain bearings. P I Mech Eng B-J Eng 226:930–940. https://doi.org/10.1177/0954405411434679
13. Liu Y, Xu N, Wang Y, Yao Y, Xiao H, Jia J, Lv H, Zhang D (2019) Preparation and tribological properties of hybrid PTFE/Kevlar fabric self-lubricating composites. Surf Coat Tech 361:196–205. https://doi.org/10.1016/j.surfcoat.2018.12.121
14. Qiu M, Liang X, Li YC, Pang XX (2016) Effects of the different modification treatment liners on tribological properties of self-lubricating spherical plain bearings and the bonding property of liners. Proceedings of 6th ICMMBE 361–366. https://doi.org/10.2991/icmmbe-16.2016.69
15. Qiu M, Miao Y, Li Y, Lu J (2015) Film-forming mechanisms for self-lubricating radial spherical plain bearings with hybrid PTFE/aramid fabric liners modified by ultrasonic. Tribol Int 87:132–138. https://doi.org/10.1016/j.triboint.2015.02.025
16. Yang Y (2011) Sliding wear of the hybrid Kevlar/PTFE fabric reinforced phenolic composite filled with Nano-titania. Chin J Mech Eng 24:154–159. https://doi.org/10.1016/j.triboint.2015.02.025
17. Zhang HJ, Zhang ZZ, Guo F (2012) Tribological behaviors of hybrid PTFE/nomex fabric/phenolic composite reinforced with multiwalled carbon nanotubes. J Appl Polym Sci 124:235–241. https://doi.org/10.1002/app.33594
18. Ren G, Zhang Z, Zhu X, Ge B, Guo F, Men X, Liu W (2013) Influence of functional graphene as filler on the tribological behaviors of Nomex fabric/phenolic composite. Compos Part A-Appl. S. 49:157–164
19. Ren G, Zhang Z, Zhu X, Men X, Liu W (2014) Influence of lubricant filling on the dry sliding wear behaviors of hybrid PTFE/Nomex fabric composite. J Mater Sci Lett 49:3716–3724. https://doi.org/10.1007/s10853-014-8081-y
20. Yang M, Yuan J, Men X, Zhang Z, Guo F, Liu W (2016) Effect of ZrB2 particles incorporation on high-temperature tribological properties of hybrid PTFE/Nomex fabric/phenolic composite. Tribol Int 99 :289–295
21. Sun W, Gu Y, Yang Z, Li M, Wang S, Zhang Z (2018) Enhanced tribological performance of hybrid polytetrafluoroethylene/Kevlar fabric composite filled with milled pitch-based carbon fibers. J Appl Polym Sci 135. https://doi.org/10.1002/app.46269

22. Zhang HJ, Zhang ZZ, Guo F (2011) Studies of the influence of graphite and MoS2 on the tribological behaviors of hybrid PTFE/Nomex fabric composite. Tribol T 54:417–423. https://doi.org/10.1080/10402004.2011.553027
23. Li H, Yin Z, Jiang D, Huo Y, Cui Y (2014) Tribological behavior of hybrid PTFE/Kevlar fabric composites with nano-Si3N4 and submicron size WS2 fillers. Tribol Int 80:172–178. https://doi.org/10.1016/j.triboint.2014.07.006
24. Ren G, Zhang Z, Song Y, Li X, Yan J, Wang Y, Zhu X (2017) Effect of MWCNTs-GO hybrids on tribological performance of hybrid PTFE/Nomex fabric/phenolic composite. Compos Sci Technol 146:155–160. https://doi.org/10.1016/j.compscitech.2017.04.022
25. Yuan J, Zhang Z, Yang M, Wu L, Li P, Guo F, Men X, Liu W (2019) Coupling hybrid of BN nanosheets and carbon nanotubes to enhance the mechanical and tribological properties of fabric composites. Compos Part A-Appl S 123:132–140. https://doi.org/10.1016/j.compositesa.2019.05.010
26. Obradović V, Simić D, Zrilić M, Stojanović DB, Usković PS (2021) Novel hybrid nanostructures of carbon nanotube/fullerene-like tungsten disulfide as reinforcement for aramid fabric composites. Fiber Polym 22:528–539. https://doi.org/10.1007/s12221-021-0278-5
27. Zhang ZZ, Zhang HJ, Guo F, Wang K, Jiang W (2009) Enhanced wear resistance of hybrid PTFE/Kevlar fabric/phenolic composite by cryogenic treatment. J Mater Sci Lett 44:6199–6205. https://doi.org/10.1007/s10853-009-3862-4
28. Huang T, Lu R, Ma Y, Liu P, Chen H, Huang Z, Li T (2012) Surface modification by air-plasma treatment and its effect on the tribological behavior of hybrid fabric-polyphenylene sulfide composites. J Macromol Sci B 51:1011–1026. https://doi.org/10.1080/00222348.2011.625877
29. Liu N, Wang J, Chen B, Han G, Yan F (2014) Enhancement on interlaminar shear strength and tribological properties in water of ultra high molecular weight polyethylene/glass fabric/phenolic laminate composite by surface modification of fillers. Mater Design 55:805–811. https://doi.org/10.1016/j.matdes.2013.10.053
30. Yuan J, Zhang Z, Yang M, Guo F, Men X, Liu W (2017) Surface modification of hybrid-fabric composites with amino silane and polydopamine for enhanced mechanical and tribological behaviors. Tribol Int 107:10–17
31. Qi X, Wang H, Dong Y, Fan B, Zhang W, Zhang Y, Ma J, Zhou Y (2019) Experimental analysis of the effects of laser surface texturing on tribological properties of PTFE/Kevlar fabric composite weave structures. Tribol Int 135:104–111. https://doi.org/10.1016/j.triboint.2019.02.036
32. Yang M, Zhu X, Ren G, Men X, Guo F, Li P, Zhang Z (2015) Influence of air-plasma treatment and hexagonal boron nitride as filler on the high temperature tribological behaviors of hybrid PTFE/Nomex fabric/phenolic composite. Eur Polym J 67:143–151. https://doi.org/10.1016/j.eurpolymj.2015.03.027
33. Wang J, Liu N, Yang J, Han G, Yan F (2016) Combined effect of chemical surface treatment of Kevlar fabric and PTFE fillers on the water-involved tribological performance of Kevlar fabric/phenolic laminate. Tribol T 59:385–390. https://doi.org/10.1080/10402004.2015.1087079
34. Yuan J, Zhang Z, Yang M, Li P, Jiang W, Zhao X, Liu W (2021) Enhanced high-temperature tribological performance of PTFE/PI fabric composites by simultaneously introducing PDA/SiO2 hybrid coating and aramid product reinforcements. Polym Compos 42:3539–3549. https://doi.org/10.1002/pc.26077
35. Wang H, Qi XW, Zhang WL, Dong Y, Fan BL, Zhang Y (2020) Tribological properties of PTFE/Kevlar fabric composites under heavy loading. Tribol Int 151:1–10. https://doi.org/10.1016/j.triboint.2020.106507
36. Xue Y, Yan S, Xie J, Feng Z, Zou J (2019) Contact and tribological properties of self-lubricating ellipsoidal plain bearings. Tribol Int 140:1–10. https://doi.org/10.1016/j.triboint.2019.105840
37. Yang M, Zhang Z, Yuan J, Wu L, Zhao X, Guo F, Men X, Liu W (2019) Fabrication of PTFE/Nomex fabric/phenolic composites using a layer-by-layer self-assembly method for tribology field application. Friction 8:335–342. https://doi.org/10.1007/s40544-019-0260-z
38. Li P, Zhang Z, Yang M, Yuan J, Jiang W (2021) Synchronously improved thermal conductivity and tribological performance of self-lubricating fabric liner composites via integrated design method with copper yarn. Tribol Int 164:1–10. https://doi.org/10.1016/j.triboint.2021.107204
39. Xue Y, Chen J, Guo S, Meng Q, Luo J (2018) Finite element simulation and experimental test of the wear behavior for self-lubricating spherical plain bearings. Friction 6:297–306. https://doi.org/10.1007/s40544-018-0206-x
40. Luo L, Wang X, Liu H, Zhu L (2018) Number simulation analysis of self-lubricating joint bearing liner wear. Int J Interact Des M 13:23–34. https://doi.org/10.1007/s40544-018-0206-x
41. Cui W, Raza K, Zhao Z, Yu C, Tao L, Zhao W, Chen W, Peng S, Xu Q, Ma L, Hu Y, Liao D, Liang B, Wang T, Ma T (2020) Role of transfer film formation on the tribological properties of polymeric composite materials and spherical plain bearing at low temperatures. Tribol Int 152. https://doi.org/10.1016/j.triboint.2020.106569
42. Tan D, Li R, He Q, Yang X, Zhou C, Mo J (2021) Failure analysis of the joint bearing of the main rotor of the Robinson R44 helicopter: a case study. Wear 477:1–11. https://doi.org/10.1016/j.wear.2021.203862
43. Woodhead J, Truman CE, Booker JD (2015) Modelling of dynamic friction in the cold forming of plain spherical bearings. Surf Contact Mech including Tribology XII, 91:141–152. https://doi.org/10.2495/SECM150131
44. Xin LL (2018) Optimal design of the process for self-lubricating spherical plain bearings based on finite element analysis. IOP Conference Series: Materials Science and Engineering 452:1–9. https://doi.org/10.1088/1757-899X/452/2/022001
45. Hu CL, Ou H, Zhao Z (2015) An alternative evaluation method for friction condition in cold forging by ring with boss compression test. J Mater Process Tech 224:18–25. https://doi.org/10.1016/j.jmatprotec.2015.04.010
46. Button ST (2012) Tribology in metal forming processes, in: Davim J. (Eds.) Tribology in manufacturing technology. Materials Forming, Machining and Tribology, Berlin, Heidelberg. pp. 103–120. https://doi.org/10.1007/978-3-642-31683-8_3
47. Bay N, Azushima A, Groche P, Ishibashi I, Merklein M, Morishita M, Nakamura T, Schmid S, Yoshida M (2010) Environmentally benign tribo-systems for metal forming. CIRP Ann 59:760–780. https://doi.org/10.1016/j.cirp.2010.05.007
48. Groche P, Kramer P, Bay N, Christiansen P, Dubar L, Hayakawa K, Hu C, Kitamura K, Moreau P (2018) Friction coefficients in cold forging: a global perspective. CIRP Ann 67:261–264. https://doi.org/10.1016/j.cirp.2018.04.106
49. Kunogi M (1956) A new method of cold extrusion. J Sci Res Inst (Tokyo) 50:215–246
50. Male AT, Cockcroft MG (1964) A method for the determination of the coefficient of friction of metals under conditions of bulk plastic deformation. J Inst Metals 9:38–46. https://doi.org/10.1016/0043-1648(66)90161-X
51. Kim H, Yoon JW, Chung K, Lee MG (2020) A multiplicative plastic hardening model in consideration of strain softening and strain rate: theoretical derivation and characterization of model parameters with simple tension and creep test. Int J Mech Sci 187:105913. https://doi.org/10.1016/j.ijmecsci.2020.105913
52. Male AT, Depierre V (1971) The validity of mathematical solutions for determining friction from the ring compression test.

Wear 17(3):389–397. https://doi.org/10.1016/0043-1648(71)90094-9
53. Tobiason FL (1990) Phenolic resin adhesives. in: Skeist I. (Eds.) Handbook of adhesives. Springer, Boston, USA. https://doi.org/10.1007/978-1-4613-0671-9_17
54. Conley RT, Bieron F (1963) A study of the oxidative degradation of phenol-formaldehyde polycondensates using infrared spectroscopy. J Appl Polymer Sci 7:171–180. https://doi.org/10.1002/app.1963.070070110
55. Sutter G, Ranc N (2010) Flash temperature measurement during dry friction process at high sliding speed. Wear 268:1237–1242. https://doi.org/10.1016/j.wear.2010.01.019
56. Ren GN, Zhang ZZ, Zhu XT, Men XH, Jiang W, Liu WM (2014) Sliding wear behaviors of Nomex fabric/phenolic composite under dry and water-bathed sliding conditions. Friction 2:264–271. https://doi.org/10.1007/s40544-014-0046-2
57. Nuruzzaman DM, Chowdhury MA (2012) Effect of normal load and sliding velocity on friction coefficient of aluminum sliding against different pin materials. Am J Sci 2:26–31. https://doi.org/10.5923/j.materials.20120201.05
58. Johnson AF, Holzapfel M (2016) Influence of delamination on impact damage in composite structures. Compos Sci Technol 66:807–815. https://doi.org/10.1016/j.compscitech.2004.12.032
59. de Borst R, Remmers JJC (2006) Computational modelling of delamination. Compos Sci Technol 66:713–722. https://doi.org/10.1016/j.compscitech.2004.12.025
60. Wang SS, Yu TP (2004) Nonlinear mechanics of delamination in fiber-composite laminates: asymptotic solutions and computational results. Compos Sci Technol 66:776–784. https://doi.org/10.1016/j.compscitech.2004.12.020
61. Friedrich K, Reinicke P (1998) Friction and wear of polymer-based composites. Mech Compos Mater 34:503–514. https://doi.org/10.1007/BF02254659